Hindcasting the 2017 dispersal of Sargassum algae in the Tropical North Atlantic

L. Berline, Anouck Ody, Julien Jouanno, Cristele Chevalier, Jean-Michel André, Thierry Thibaut, Frédéric Ménard

HAL Id: hal-02925638

https://hal.archives-ouvertes.fr/hal-02925638

Submitted on 30 Aug 2020

Hindcasting the 2017 dispersal of *Sargassum* algae in the Tropical North Atlantic

Léo Berline*[1], Anouck Ody*[1], Julien Jouanno[2], Cristèle Chevalier[1], Jean-Michel André[1], Thierry Thibaut[1], Frédéric Menard[1]

* Equal contribution
[1] Aix Marseille Univ., Universite de Toulon, CNRS, IRD, MIO UM 110 , 13288, Marseille, France
[2] LEGOS, Université de Toulouse, IRD, CNRS, CNES, UPS, Toulouse, France

Abstract

Since 2011, huge amounts of *Sargassum* algae are detected in the equatorial Atlantic, causing large strandings events on the coasts of the West Indies, Brazil and West Africa. The distribution of this stock shows strong annual and interannual variability, whose drivers are not settled yet. Here we use satellite *Sargassum* observations from MODIS and currents from an ocean reanalysis to simulate the passive transport of algae in 2017. Wind effect was necessary to fit the observed distribution. Simulations reasonably reproduce the satellite monthly distribution for up to seven months, confirming the prominent role of transport in the distribution cycle. Annual cycle appears as a zonal exchange between eastern (EAR) and western accumulation regions (WAR). EAR is well explained by advection alone, with sharp meridional distribution controlled by converging currents below the inter-tropical Convergence Zone. Instead, WAR is not explained by advection alone, suggesting local growth.

Highlights:
- Windage from 0,5 to 2% of wind velocity improved predicted distribution of Sargassum
- Prominent role of transport in the annual cycle of distribution
- Eastern accumulation region due to slowing down of North Equatorial Counter Current, with high retention
- Western accumulation region due to circulation in the North Brazil Current system, and possibly growth

Introduction

In 2011, massive strandings of holopelagic *Sargassum* algae occurred on the coasts of the Lesser Antilles, northern Brazil and West Africa (Franks et al. 2011, de Széchy et al 2012, Oyesiku and Egunyomi 2014). The same year, satellites detected above normal floating algae coverage over a vast area evolving over the major part of tropical and equatorial Atlantic (Gower et al 2013), suggesting that localized stranding events were only the visible part of a large offshore stock. Since 2011, *Sargassum* inundations repeated every year except 2013 (Wang & Hu 2016, Wang et al 2019).

Investigating such a large scale phenomenon involves integrating physical and biological processes, namely the physical transport of floating algae and its growth in response to changing oceanic conditions (e.g. temperature and nutrients, see Djakoure et al (2017), Wang & Hu 2016 and Wang et al (2019)).

The first question addressed was the source of these stranded algae. Starting from *Sargassum* stranding locations recorded in 2011, backward in time particle tracking simulations identified the potential source region as being the Equatorial Atlantic (Franks et al 2011). Based on these findings, Franks et al, (2011) postulated that *Sargassum* are circulating in a large recirculation region bounded by the South Equatorial current (SEC) to the south and the North Equatorial Counter Current (NECC, see Lumpkin and Garzoli (2005) for instance) to the North, so-called NERR (North Equatorial recirculation region). Franks et al (2016) further refined his hypothesis using observed surface buoys trajectories and particle tracking experiment simulations. They proposed a clockwise circulation of *Sargassum* with two consolidation regions, in the eastern and western ends of the NERR. In Spring, *Sargassum* would escape from the NERR to drift toward the Caribbean.

The link between the western consolidation region (renamed Central West Atlantic, CWA) and the abundance in the Caribbean was supported by Wang & Hu (2017) using satellite detection time series. They showed that abundance in the CWA in February correlated well with abundance in the Caribbean three

months later. Building on this hypothesis, Putman et al (2018) used forward and backward particle tracking simulations based on HYCOM reanalysis to explore the role of oceanic transport in the link between *Sargassum* abundance in the CWA and in the Caribbean Sea. They confirmed that the majority of particles released in the CWA eventually enter the Caribbean. However, transport alone could not explain the fluctuations of *Sargassum* abundance in the Caribbean over the period 2000-2015.

Apart from transport, growth is the other factor invoked to explain *Sargassum* fluctuations. Brooks et al (2018) built a model including *Sargassum* transport and physiology. They showed that including growth is necessary to simulate persistent abundance in the tropics as well as in the North East Atlantic. They analyzed a climatological year and did not focus on the tropical region.

Recently, Wang et al (2019) extended satellite detections for the tropical Atlantic region over 2000-2018. They showed that the distribution pattern of 2011 is repeating and increasing in amplitude. Based on Lagrangian simulations over a climatological year, they concluded that transport largely explain the so called 'belt' summer distribution. Combining their dataset with complementary satellite and *in situ* data, they put forward new hypothesis for the onset of this *Sargassum* belt and for causes of interannual fluctuations. In particular, they point out a potential effect of the West African upwelling and the 'seeding' effect of remaining winter biomass on the next year. Lately, Johns et al (2020) identified vertical mixing, open ocean upwelling and upwelling in the Guinea Dome as the key nutrient sources for *Sargassum* growth. Most importantly, Johns et al (2020) argue that the new tropical *Sargassum* population results from a large scale dispersal event that occurred in 2010, driven by anomalous westerly winds.

While transport appears as an important driver, a detailed analysis of the role of advection by equatorial currents in shaping the distribution through the year is missing. Here, using satellite data and synoptic Lagrangian simulations, we first validate the role of transport over 2017, then propose an analysis of this typical high *Sargassum* year, focusing on the main *Sargassum* transport pathways, fluxes and regions of aggregation, over one annual cycle.

Materials and Methods

Our strategy was to use satellite derived algal presence index to initialize and validate Lagrangian simulations. First the satellite products are described, then the simulations.

Satellite detection of *Sargassum*
To detect *Sargassum* from satellite, maps of alternative Floating Algae Index (AFAI, Wang & Hu 2016) were computed using MODIS Aqua and Terra satellites. The full description of the processing chain, modified from Wang & Hu 2016, is given in supplementary material. The output of the chain is a map of AFAI with a resolution of 0.01° for the North Atlantic from 0° to 40°N for each day of 2017. *Sargassum* presence was detected by AFAI > 5E-4 sr-1. This threshold value was chosen based on the analysis of our 2017 AFAI dataset and allowed to isolate main *Sargassum* aggregations. It is worth noting that actual *Sargassum* presence was supported by in situ observations made during two cruises over the Tropical Atlantic in 2017 (Ody et al, 2019).

Compositing
On a daily AFAI map, the average number of pixel containing *Sargassum* is low due to extensive cloud masking and to the nature of *Sargassum* aggregation: south of 25°N, on average ~20 % of pixels were not masked, among which only ~15 % were detected as containing *Sargassum*. Therefore to get a robust statistical estimate, a compositing over one month and 50km square cells was achieved, similar to Wang & Hu 2016 (one month, 0,5° square cells). In each 50km cell, the proportion p of pixels containing *Sargassum* (Ns) with respect to the number of unmasked pixels (Nu) was computed for each day (p=Ns/Nu), then averaged for the month. Thus p neglects the actual *Sargassum* coverage within a pixel (i.e. fractional coverage equals 0 or 1), but this is sufficient as we are not aiming at quantifying biomass Finally, these composites were screened to keep only the regions with relevant detections: Cells with *p<0.3%* corresponding to isolated aggregations were set to 0 and cells with p>0,3% for less than two successive days were considered as false detection and removed. This last product will be referred to as satellite monthly composite.

Lagrangian simulations

   1) Velocity and wind fields

Velocity fields were outputs extracted from a 1/12° resolution simulation carried out with PSY4V3R1 global configuration provided by MERCATOR-OCEAN (Lellouche et al 2013). This configuration was forced by realistic surface fluxes from ECMWF and included surface and vertical profiles data assimilation. Vertical resolution was ~1m near the surface. Daily averages of velocity fields were used. Comparison with surface drifters in the equatorial Atlantic reveals a slight overestimation of magnitude but no bias in direction (Lellouche et al 2013). Windage component was computed using 10m above surface winds from ECMWF HRES (Owens and Hewson. 2018).

2) Particle tracking

To simulate the drift of *Sargassum* aggregations, Lagrangian particle trajectories were computed. As pelagic *Sargassum* algae float at the sea surface (Butler et al 1983), particles were kept in the model top layer. Particle advection was carried out using Runge Kutta 4th order numerical scheme implemented in the Ichthyop lagrangian software (Lett et al 2008), with a time step of 1800s. The velocity field was linearly interpolated in space and time. Particle positions were saved every 12h. When a particle approached a lateral boundary (coast), it "bounced", so that no particles were lost from the simulations. Bouncing was chosen because (i) the hydrodynamic model resolution (~8km) is too coarse to resolve coastal and nearshore processes that lead to stranding and (ii) to be conservative on the number of active particles representing *Sargassum* cover, To assess the sensitivity to the bouncing boundary condition, test simulations were also run with beaching behavior (particle is removed from simulation when it approaches the coast). Direct wind effect on particle drift was tested, taking into account a windage component added to the ocean velocity. Here windage is a simple correction meant to to represent real windage (direct wind draft on *Sargassum* emerged parts), but also residual momentum due to waves (Stockes drift) not accounted for by the circulation model and to compensate for underestimation of the surface Ekman component, by the circulation model. While oil slicks were observed to drift at 3,5% of wind speed (*Schwartzberg*, 1971), paired trajectories between *Sargassum* aggregation and SVP buoy (Supplementary material) suggested a windage similar to that used for undrogued SVP drifting buoys, e.g. 1% of the wind velocity following Poulain et al (2009). However, as the optimal windage is unknown, values between 0 and 2% were tested by computing the fit to the satellite observations.

3) Simulations set up

Our approach was to hindcast the distribution of observed *Sargassum* aggregations assuming passive transport. We first simulated the month-to-month drift of observed *Sargassum* aggregations present in the satellite monthly composites (Exp 1). Each 50km cell with $p>0$ was seeded by an ensemble of $N_0=625$ particles (one every 2 km). A sensitivity analysis showed that increasing N_0 did not changed significantly the results. To take into account the proportion p of *Sargassum* in each cell ($0<p<0.2$), each particle is associated to a weight equal to $w=p/N_0$, representing a discrete *Sargassum* cover. This weighting allowed keeping the same number of particles per cell while considering varying values of p. Using this approach, each satellite monthly composite was converted into initial particle positions. From these initial particle positions, starting on the 15th of month j, simulations were run until the end of month j+1 (44 to 47 days depending on the month). With this approach, the initial observation time and location were approximated. A total of 11 simulations were performed, to cover the months from February to December of 2017.

In addition, using the same times and initial particle positions, one year simulations (Exp2) were carried out by looping on the velocity outputs from 2017, allowing to study long term advection and the full annual cycle. Finally, to identify regions of aggregation by currents, one month simulations were carried out with homogeneous seeding (1 particle every 5 km, Exp3). Test simulations with beaching behavior were also run as for Exp2. These experiments are summarized in table 1.

Experiment	Duration	windage	Initial positions
Exp1	45 days from 15th month j to end month j+1	variable	Satellite composite month j, j=January to November
Exp2	350 days from 15th month j to end month j-1 2018	variable	Satellite composite month j, j=January to December
Exp3	45 days from 15th month j to end month j+1	1%	Homogeneous (1 particle/5km over 5°S-25°N)

Table 1. Lagrangian experiments set up.

3

4) Conversion from ensemble particle trajectories to simulated monthly composites

Daily positions of particles during month j+1 were used to compute the total weight of particle present in each 50 km cell (same cells as the AFAI monthly composites, p_cell= $\sum \left(w_i \right)$ for i particles contained in the cell), resulting in daily density maps. Then, these maps were composited for each month by averaging all daily density maps, producing a simulated monthly composite. Note that, for month-to-month simulations the cloud masking present on daily AFAI maps was applied to our simulated daily density maps. To do so, for each daily density map, each cell with Nu=0 (fully masked) on the corresponding daily AFAI map was not taken into account in the average. The simulated monthly composite for month j+1 can then be compared to the satellite monthly composite of month j+1. For Exp2, no cloud masking was applied.

5) Skill diagnostics

To compare the *Sargassum* spatial distribution shown by the satellite and simulated monthly composites, we use the True Skill Statistic (TSS, Allouche et al 2006) that allows to quantify the match between two presence-absence fields. TSS balances the advantages of sensitivity and specificity, a TSS value of 1 meaning a perfect fit. As the region of occurrence of *Sargassum* is limited to the tropical Atlantic, TSS is only computed from 0 to 25°N. We chose this diagnostic rather than correlation because correlation is not adapted to compare data with numerous null (absence) values. Moreover, the absolute value *p* at each cell is difficult to compare between satellite and simulated composites for simulations lasting several months, due to the absence of growth processes.

For long simulations (Exp2), the particles tend to disperse with time leading to a strong decrease with respect to the initial particle density. To compensate for this dispersal due to numerical diffusion and to the absence of growth and mortality processes, we chose to scale linearly the simulated *p*-values to match the satellite values (scaled_p_sim=p_sim*max(p_sat)/max(p_sim)). Low p-values (<0,3 %) were also removed to be consistent with satellite composites. Then all *p*-values > 0 were considered as presence for satellite and scaled simulated composites and used for TSS. For month to month simulations (Exp1), no scaling was applied. As a TSS of 1 cannot be expected, we computed a reference TSS value to quantify the added value of our simulated composites. This reference TSS was computed between successive satellite composites (month j+1 and month j) and called persistence, as the forecast is simply a constant field in this case.

6) Fluxes

To quantify the different pathways taken by *Sargassum*, fluxes of particles were computed using the annual simulations (Exp2), taking into account the weights associated to particles. Four regions were defined by dividing the basin zonally at 55°W, 30°W and 8°W: Caribbean Sea, Central Atlantic, East Atlantic and Gulf of Guinea. We focused on the fate of *Sargassum* aggregations observed (i) in the Central Atlantic between 55-30°W in spring (April to July) and (ii) in the East Atlantic between 30-8°W and 5-13°N in fall (August to December). Proportion of retention and exchanges between these regions were computed for trajectories integrated over 6 months periods, which corresponds to the time scale of zonal transport across the basin. Monthly and period averages were computed.

Results

1. Annual evolution of *Sargassum* distribution

Considering the total coverage over the whole domain (Fig 1), an annual cycle was observed with a low *Sargassum* coverage in winter, increasing after March and peaking in July. Then a sharp decrease of coverage occurred in the fall, with coverage returning to a low value in December, similar to January.

We now describe the evolution of *Sargassum* aggregations from satellite observations together with surface model currents (Fig 1). In January, two aggregations were visible, one (noted A) centered around 40°W 13°N, the other (noted B) covering 20-30°W, 2-9°N. From January to February, displacement of aggregations A and B was westward covering approximately 3° in longitude. Aggregation A drifted with the North Equatorial Current (NEC), while aggregation B drifted with the northern branch of the South Equatorial Current (nSEC) along 4-5°N. In March, aggregation A partly vanished while aggregation B continued its westward spread along 4°N with a tongue at ~ 26°W. in May, it widened off Brazil, in the recirculation region

between nSEC and North Brazil Current (NBC). Its tail was displaced northward and meandered with Tropical Instability Waves (TIW). In June, *Sargassum* aggregations spread toward east and west forming a belt, reaching the Caribbean islands in the west through transport by NBC and extending east toward Africa with the onset of the NECC along 7°N. July was the month of maximal zonal spread along 7-9°N. Aggregation entered the Caribbean Sea, then the south subtropical gyre in August. In July-October, north and eastward drift by the NBC retroflection and intensifying NECC along 5-7°N brought *Sargassum* along West Africa where it accumulated. The *Sargassum* belt meandered with the large instability waves except the part near Africa east of 20°W. In September, the western tail disappeared in the Caribbean Sea and subtropical gyre. Finally in November-December the center of aggregation B drifted north, where it was taken back by westward flowing NEC along 11-12°N. A new center aggregation (noted A') appeared at ca 43°W. In December, the annual cycle was closed with the aggregation A' drifting west, similar to aggregation A in January. Large aggregations were often observed on the edges of the main currents, not in their core, as for instance the aggregation B off Brazil in April, bounded by NBC and nSEC, and aggregation off West Africa in September bounded by NECC to the north.

2. Overall performance of simulations and choice of optimal windage.

The overall fit of simulations with respect to observations was analyzed using TSS. One-month simulations (Exp1) showed TSS values from 0.4 to 0.8 (Fig 2A), while TSS for persistence varied from 0.3 to 0.6. TSS for persistence illustrated that distribution changed rapidly in winter and spring, and was more stable in summer and fall. Simulations were much better than persistence during winter and spring, then this difference decreased in summer and fall, with a minimum in October and November. Adding 1% windage improved the mean TSS from 0.58 to 0.64. 1% windage produced the best fit, but differences among windage values were small.

For longer simulations (Exp2), most TSS curves decreased with time without windage because of particles drifting north, out of the area of *Sargassum* detection (Fig 2B). With 1% windage, TSS values were much higher (Fig 2C) and comparable to Exp1 for most of the year. Simulations initialized in January-February-March showed a decrease of TSS followed by an increase during summer months, similar to the TSS pattern of Exp1. Among windage values, 1% windage produced the best fit (0.65 on average against 0.48 for no windage, Fig S1).

In the 1% windage case, distributions were better than persistence except in the fall for the January initialization. Adding windage mainly resulted in a reduced northward transport of particles. Indeed, trade winds added a southwestward component to the current velocity, which helped maintaining particles in the tropics and drove particles further west to the Caribbean Sea and Gulf of Mexico (as shown on Figs 3, 4, 5, 6). Without windage, particles tended to be transported more rapidly northward into the subtropical gyre. As 1% windage produced the best fit, from now on only simulations using this value are analyzed.

Regarding the spatial distribution, one month simulations (Exp1) show an annual evolution fully consistent with satellite (Fig 3, right panel), although simulated aggregations were on average slightly more extended than in satellite composites. In several occasions, aggregations disappeared in observations while simulations maintain it: Aggregation A (40°W, 15°N) in March, aggregation off West Africa (15°W, 9°N, off Liberia) in November and also in the Caribbean Sea in August. Considering longer simulations (Exp2), we observed the closing of the annual cycle from December 2017 to January of the next year (Figs 5 and 6). Accumulation off Africa in December fed the new aggregation in the central Atlantic, transported westward by NEC along 11°N and by TIW toward the south, taken back by the nSEC.

3. Exchange of *Sargassum* across the basin and aggregation

Regarding the fluxes of *Sargassum*, only 9 % of the *Sargassum* observed in the West Atlantic in April reached the Caribbean area within 6 months (20 % within a year) (Fig 7A). 79 % turned back toward East Atlantic forming the *Sargassum* accumulation observed off Africa in fall, and 12 % remained in the Central Atlantic. Of the eastern accumulation observed in October, 37% of *Sargassum* remained in the East Atlantic, 32% reached the Gulf of Guinea and the remainder (30 %) drifted westward to Central Atlantic (Fig 7B). Similar figures were obtained when computing fluxes for spring and fall period.

When particles were initialized homogeneously (Exp3, Fig 8), regions of persistent dispersal and aggregation appeared. Persistent equatorial divergence emptied particles south of 3°N. A belt of aggregated particle appeared at latitudes 6 to 8°N bounding nSEC then NECC to the north, moving northward during the year,

consistent with the observations. Along West Africa, *Sargassum* aggregated from May to October, consistent with the observations. In the western part of the basin, aggregations were more transient than in the east, with the largest aggregations occurring in August-October associated to the NBC retroflection, later than the observations. In the Gulf of Guinea, simulations produced year-round aggregation between Guinea Current and nSEC, less intense in summer. This aggregation was absent in the observations.

Discussion

1. Role of transport, growth and losses

Regardless of the total coverage, the annual cycle appears as an alternation of westward transport in January-March, then spreading zonally and northward as a belt from Caribbean to Africa, finally accumulating along West Africa in the fall.

Month to month simulations (Exp1) well reproduce the dispersal pattern shown by satellite, although with a tendency to overestimate the spread of *Sargassum*. This discrepancy is partly linked to the time and spatial offset introduced by initial positions pooling together *Sargassum* detections over one month and over 50km square bins. Also, monthly composite may misestimate the actual presence of *Sargassum*. Satellite detection is limited by signal to noise ratio (Wang & Hu 2016), heavy cloud coverage typical of tropical region, and sea-state. However, we believe that our approach is well suited for our basin scale study, not focusing on the drift of individual aggregations but on the main routes of transport of the major aggregations.

For long simulations (Exp2), south of 15°N the dispersal stays consistent with 2017 observations up to 7 months ahead, but the agreement with satellite depends on the starting month. Comparison is better for simulations starting in spring. These results show that transport is the dominant driver of the annual evolution of *Sargassum* spatial distribution, and that we can use it to forecast distribution several months in advance. They extend the findings of Wang et al (2019) that focused on the January-July period of a climatological year, using HYCOM currents and a 1% windage. Compared to other years (Wang et al 2019, their movie S1), the annual evolution of 2017 is similar to the high *Sargassum* years 2011-2018 except 2013. This regularity is consistent with the strong forcing of the circulation on the *Sargassum* distribution. However, there is interannual variability. In January 2011 and 2014, the aggregation A was absent. When present, this aggregation can persist and reach the Caribbean as early as March-April, as in 2015 and 2018, or partly vanish as in 2016 and 2017.

While transport is driving the distribution, fluctuations in total coverage indicates that processes not included in our simulations -growth and losses- are acting. For simulation starting in January, an aggregation develops north of 15°N in the subtropical gyre, absent in the observations (Fig 4 and supplementary figure S2). Also, simulations starting in January and March (Figs 4 and 5, and supplementary figures S2 and S3) miss the increase in coverage from March to July in the Western tropical Atlantic shown by observations. This may indicate that growth processes may be acting south of 10°N, while loss processes may be acting in the southern subtropical gyre.

As we only have satellite observations, apparent growth and loss shown by satellite observations may be caused by processes acting at very different scales, from the individual algae up to the raft aggregation. Some *Sargassum* aggregations vanish in the satellite record while simulations maintain it. This may result from actual disappearance by sinking of *Sargassum* algae, resulting from wind mixing, senescence, or from satellite detection being limited by sea-state. Indeed *In situ*, after strong wind (>7m/s), subsurface *Sargassum* and disaggregated raft were observed by Ody et al (2019). Aggregation A (40°W, 15°N) disappears in March while simulations keep it unchanged. Wind may be the reason, as from February 15th to March 31st, there was 7 days of wind >10m/s in the region of the aggregation. Again in the Caribbean Sea, when aggregation drops in August, wind >10m/s was observed during 6 days in the area. This suggests that wind is an important factor impacting *Sargassum* detection, and maybe *Sargassum* survival. This wind effect would have to be considered in a forecasting context.

In the Gulf of Guinea, loss processes may be different. Indeed, in the eastern accumulation region, off West Africa (15°W, 9°N, Fig 1) currents advect algae toward the Gulf of Guinea during September-October, where no *Sargassum* are detected. Moreover this aggregation shows a drop in coverage from October to November while simulations keep it unchanged. There, wind was weak (<5m/s) and no strong average current was simulated. This apparent loss may then be linked to senescence, or to dispersal in absence of aggregation processes. Stranding on the coast is another missing process that may contribute to the

observed loss. However, test simulations using beaching behavior (supplementary figure S5) showed that it has a negligible impact on simulated distributions (less than 1% change in TSS). Further, less than 0,25% of the initial particles beached after one year, whatever the starting month. Thus, as far as the simulated beaching can be trusted, beaching does not appear as a significant loss term.

2. *Sargassum* transport pathways in the equatorial region.
Franks et al (2016) proposed an anticyclonic circulation of *Sargassum* in the Northern equatorial band, with two "consolidations regions". These consolidation regions are confirmed here, For the transport routes, several points differ from Franks et al (2016) (Fig 1). In 2017, the western accumulation shown by observations is associated with a cyclonic recirculation located between nSEC and NBC, not directly to NBC retroflection as proposed before. The main westward route is along 4-5°N corresponding to nSEC. An additional westward route along 13°N in January-February can appear, which was also present in 2015 and 2018. The closing of the annual cycle from December to January consists in a re-seeding of the central Atlantic from the eastern accumulation region (Figs 5, 6), through NEC transport and TIW. This re-seeding may determine abundance during the next year, as suggested by Wang et al (2019).

3. Role of aggregation and fluxes
Simulations initialized from homogeneous distribution (Exp3, Fig 8) revealed the key role of converging surface circulation below the Inter Tropical Convergence Zone (ITCZ) in shaping the *Sargassum* distribution. Regions of *Sargassum* detection correspond in general (60% of cases) to regions where transport accumulates particles, ie convergence regions. This is the case of the zonal belt appearing in June-July bounded by the nSEC and the NECC, and of the eastern accumulation region which develops at the termination of the NECC. This is also consistent with observations showing satellite aggregations mostly located at the edge of currents (Fig 1). Surface convergence is driven by wind convergence under the ITCZ as shown by Johns et al (2020), and by zonal currents. However detection can occur outside of simulated convergence regions, as for instance aggregation A. This indicates that aggregations formed in a convergence region can be transported far from this initial location by large or mesoscale circulation without being dispersed. More strikingly, the western accumulation region (west of 30°W) present in observations in April-May 2017 and across all high *Sargassum* years (see Wang et al 2019) is not characterized by presence of large aggregation in Exp3. There, simulated aggregations are transient and large aggregations appear later than in observations (June-September instead of May-June). If model circulation is realistic, this may indicate that the western accumulation region shown by satellite is due to local growth, or to continuous inputs from neighboring source regions, rather than to advection. Nutrients sustaining this growth would come from vertical mixing and open ocean upwelling north of ITCZ according to Johns et al (2020). One other possibility is that actual *in situ* aggregation occur at smaller scales that those present in the model velocity field. Simulated aggregations cover a much larger area than satellite detection. In particular, simulations produce a year-round aggregation in the Gulf of Guinea, completely absent in the observations. Particles aggregated there are mostly coming from the south (not shown), which indicates that these sources are absent. But this may also mean that some loss processes must be taken into account (senescence).

The results from Exp3 clearly show that surface circulation alone can create persistent aggregation, in particular in the East Atlantic and over shorter periods in the West Atlantic. Studying the fluctuations of the surface circulation is thus also important to interpret *Sargassum* fluctuations.

Computed *Sargassum* fluxes (Fig 7) illustrates the contrast in the dynamics of the two accumulation regions. In the western accumulation region, *Sargassum* present in April mostly ends in the eastern Atlantic (79%, 64% for spring), while only a small part ends in the Caribbean (9% in April, 16,7% for spring). This 16,7% is consistent with Putman et al (2018) results for spring (their Fig. 5), taking into account interannual variability On the contrary, the eastern accumulation region recycles 37% of its October *Sargassum* stock (respectively 45% for fall), and only exports 30% westward and 32% toward Gulf of Guinea (respectively 30 and 16% for fall), therefore acting as a buffer area with high retention. Considering absolute values, *Sargassum* fluxes (in units of km^2 of presence) toward the Caribbean are 30% larger than fluxes toward the Gulf of Guinea (respectively 2,46 10^6 km^2 and 1,89 10^6 km^2 over spring and fall). One key area of future investigation is how fluctuations of the circulation in the western tropical Atlantic modulate the *Sargassum* quantity advected toward the Caribbean and eventually cause massive strandings.

4. Role of windage

Adding windage of 1% gave the best fit to observations, especially for simulations over several months (Exp2), by limiting the northward transport of particles out of the tropical Atlantic. Wang et al (2019) also used

1% windage inspired by oil slick drift modeling. First, it is worth noting that this optimal windage may be specific to the velocity field we are using here (PSY4V3R1, MERCATOR-OCEAN). Second, this improved fit does not provide an unambiguous support for wind effect on *Sargassum* transport, as other processes may also keep more biomass in the equatorial Atlantic. For instance, Brooks et al (2018) has shown that including growth in the model also maintain biomass in the equatorial region. Putman et al (2018), using HYCOM reanalysis, also found that support for windage was non-conclusive as including windage improved the fit with regard to observed satellite surface cover but decreased the fit with respect to beaching events. This calls for an *in situ* study of raft drift taking into account *Sargassum* characteristics (depth, buoyancy, drag, etc) together with synoptic measurements of wind and surface currents (e.g. Olascoaga et al 2020).

Conclusions

This study examined the role of physical transport in the annual distribution of *Sargassum* detected by satellite over one single year. Sensitivity analysis showed that including a direct wind effect was necessary to fit the observed distribution, by maintaining *Sargassum* in the equatorial region, optimal windage being 1% of wind velocity. Simulations using this windage were able to reproduce the key features of the monthly distribution observed by satellite, for one month simulations but also over longer simulations of up to 7 months. Our simulations confirm the prominent role of transport in the annual cycle of distribution observed by satellite, while growth and loss processes can modify the quantity of *Sargassum* transported. This transport cycle appears as a zonal exchange between two accumulation regions, located in the western and eastern equatorial Atlantic with some export towards the Caribbean Sea (~17% of spring stock) and Gulf of Guinea (~16% of fall stock). The eastern region acts as a buffer area, with significant retention of *Sargassum* in the region (~45% for fall). In contrast, in the western region, aggregations are mainly exported toward the east (64% for spring) with few remaining in the region (18% for spring). Numerical experiments with homogeneous initialization predict aggregation regions consistent with the eastern accumulation region, driven by the slowing down of NECC and wind convergence. Instead, the western accumulation region is not well reproduced by these experiments, which suggests that this western *Sargassum* accumulation is due to other mechanisms, such as local growth or inputs from neighboring sources. Future studies will have to test these findings over several years. Also, *in situ* studies are needed to better quantify *Sargassum* drift and physiology.

Acknowledgments

References

Allouche, O., Tsoar, A., & Kadmon, R., 2006. Assessing the accuracy of species distribution models: prevalence, kappa and the true skill statistic (TSS). *Journal of applied ecology*, *43*(6), 1223-1232.

Brooks MT, Coles VJ, Hood RR, Gower JFR., 2018 Factors controlling the seasonal distribution of pelagic *Sargassum*. Marine Ecology Progress Series.;599: 1–18. doi:10.3354/meps12646

Butler JN., 1983. Studies of *Sargassum* and the *Sargassum* community. St Georges, Bermuda: Bermuda Biological Station for Research.

De Széchy, M. T. M., Guedes, P. M., Baeta-Neves, M. H., & Oliveira, E. N., 2012. Verification of *Sargassum* natans (Linnaeus) Gaillon (Heterokontophyta: Phaeophyceae) from the Sargasso Sea off the coast of Brazil, western Atlantic Ocean. *Check List*, *8*(4), 638-641.

Djakouré, S., Araujo, M., Hounsou-Gbo, A., Noriega, C., and Bourlès, B., 2017 On the potential causes of the recent Pelagic *Sargassum* blooms events in the tropical North Atlantic Ocean, Biogeosciences Discuss., https://doi.org/10.5194/bg-2017-346.

Franks JS, Johnson DR, Ko D-S, Sanchez-Rubio G, Hendon JR, Lay M., 2011. Unprecedented influx of pelagic *Sargassum* along Caribbean island coastlines during summer 2011. Proceedings of the 64th Gulf and Caribbean Fisheries Institute. Puerto Morelos, Mexico; pp. 6–8.

Franks, J. S., Johnson, D. R., & Ko, D. S., 2016. Pelagic sargassum in the tropical North Atlantic. *Gulf and Caribbean Research*, *27*(1), SC6-SC11.

Gower J, Young E, King S., 2013 Satellite images suggest a new *Sargassum* source region in 2011. Remote Sensing Letters. 4: 764–773. doi:10.1080/2150704X.2013.796433

Johns, E. M., Lumpkin, R., Putman, N. F., Smith, R. H., Muller-Karger, F. E., Rueda, D., ... & Werner, F. E.

(2020). The establishment of a pelagic Sargassum population in the tropical Atlantic: biological consequences of a basin-scale long distance dispersal event. *Progress in Oceanography*, 102269.

Lellouche JM, Le Galloudec O, Drévillon M, Régnier C, Greiner E, Garric G, et al., 2013 Evaluation of global monitoring and forecasting systems at Mercator Océan. Ocean Science. *9*(1), 57.

Lett, C., Verley, P., Mullon, C., Parada, C., Brochier, T., Penven, P., & Blanke, B., 2008. A Lagrangian tool for modelling ichthyoplankton dynamics. *Environmental Modelling & Software*, *23*(9), 1210-1214.

Lumpkin, R., & Garzoli, S. L., 2005. Near-surface circulation in the tropical Atlantic Ocean. *Deep Sea Research Part I: Oceanographic Research Papers*, *52*(3), 495-518.

Ody A., Thibaut T., Berline L. et al, 2019. From *in situ* to satellite observations of pelagic *Sargassum* distribution and aggregation in the Tropical North Atlantic Ocean, PlosONE, 10.1371/journal.pone.0222584

Olascoaga, M.J., Beron-Vera, F.J., Miron, P., Triñanes, J., Putman, N.F., Lumpkin, R. and Goni, G.J., 2020. Observation and quantification of inertial effects on the drift of floating objects at the ocean surface. Physics of Fluids, 32(2), doi :10.1063/1.5139045

Owens RG, Hewson T., 2018. ECMWF Forecast User Guide. Available: https://software.ecmwf.int/ wiki/display/FUG/Forecast+User+Guide

Oyesiku, O. O., & Egunyomi, A., 2014. Identification and chemical studies of pelagic masses of *Sargassum* natans (Linnaeus) Gaillon and S. fluitans (Borgessen) Borgesen (brown algae), found offshore in Ondo State, Nigeria. *African Journal of Biotechnology*, *13*(10).

Poulain, P. M., Gerin, R., Mauri, E., & Pennel, R., 2009. Wind effects on drogued and undrogued drifters in the eastern Mediterranean. *Journal of Atmospheric and Oceanic Technology*, *26*(6), 1144-1156.

Putman NF, Goni GJ, Gramer LJ, Hu C, Johns EM, Trinanes J, et al., 2018. Simulating transport pathways of pelagic *Sargassum* from the Equatorial Atlantic into the Caribbean Sea. Progress in Oceanography. 165: 205–214. doi:10.1016/j.pocean.2018.06.009

Schwartzberg, H. G. (1971), The movement of oil spills, Int. Oil Spill Conf. Proc., 1971(1), 489– 494,

Wang M., Hu C., 2016. Mapping and quantifying *Sargassum* distribution and coverage in the Central West Atlantic using MODIS observations. Remote Sensing of Environment. 2016; doi:10.1016/j.rse.2016.04.019

Wang M., Hu C., 2017. Predicting *Sargassum* blooms in the Caribbean Sea from MODIS observations. Geophysical Research Letters. 44: 3265–3273. doi:10.1002/2017GL072932

Wang, M., Hu, C., Barnes, B. B., Mitchum, G., Lapointe, B., & Montoya, J. P., 2019. The great Atlantic *Sargassum* belt. *Science*, *365*(6448), 83-87.

1
2
3
4
5
6
7
8
9
10
11
12
13
14
15
16
17
18
19
20
21
22
23
24
25
26
27
28
29
30
31
32
33
34
35
36
37
38
39
40
41
42
43
44
45
46
47
48
49
50
51
52
53
54
55
56
57
58
59
60
61
62
63
64
65

Figure captions

Fig 1. *Sargassum* monthly distribution in 2017 expressed as the proportion of pixels containing *Sargassum*. Satellite monthly composite with monthly average model surface currents overlaid as black vectors.

Fig 2. Skill diagnostic of simulations. A) Exp1. Comparison between simulated monthly composite and satellite monthly composite at month j+1 for different windage values, from February to December 2017. The TSS for persistence is in grey. B) and C) Exp2. Comparison between simulated monthly composite and satellite monthly composite, for long simulations, initialized from February to December 2017. No windage (B) and 1% windage (C). The TSS for persistence is in grey.

Fig 3. Observed and simulated *Sargassum* monthly distribution in 2017 expressed as the proportion of pixels containing *Sargassum*. Simulations show *Sargassum* distribution forecast from observations made in the previous month (Exp1). Satellite monthly composite (left column), simulated monthly composite (middle) and simulated monthly composite including 1% windage (right column). The initial positions for Lagrangian simulations are taken from the satellite monthly composite for each month from January to November 2017.

Fig 4. Observed and simulated *Sargassum* monthly distribution in 2017 expressed as the proportion of pixels containing *Sargassum*. Simulations show *Sargassum* distribution forecast from observations made in January (Exp2). Satellite monthly composite (left column), simulated monthly composite (middle) and simulated monthly composite including 1% windage (right column).

Fig 5. Same as Fig 4. with simulations starting from observations made in March (Exp2). Note that for the period after December 2017, year 2017 is repeated for currents and satellite monthly composites.

Fig 6. Same as Fig 4. with simulations starting from observations made in June (Exp2).Note that for the period after December 2017, year 2017 is repeated for currents and satellite monthly composites.

Fig 7. Main pathways of *Sargassum* to the 4 zonal regions (see text) and fluxes over 6 months drift from Exp2. The envelope of *Sargassum* trajectories is shown, with the thickness of the central line following the percentage of *Sargassum* reaching the region after 6 months. A) Pathways of Central Atlantic *Sargassum* in April, B) Same as A) for *Sargassum* present in the East Atlantic in October.

Fig 8. *Sargassum* monthly distribution in 2017, starting from homogeneous initial positions (Exp3). The background color is the ratio between final and initial density, in %. The red contour lines overlaid correspond to the area of *Sargassum* presence from satellite monthly composite.

Supplementary figures:

Fig S1 Average TSS for different windage values (Exp2).
Fig S2 Same as figure 4 with no scaling applied to the simulated monthly composites. Note the narrow range of scalebar.
Fig S3 Same as figure 5 with no scaling applied to the simulated monthly composites. Note the narrow range of scalebar.
Fig S4 Same as figure 6 with no scaling applied to the simulated monthly composites. Note the narrow range of scalebar.
Fig S5 Average *Sargassum* beaching distribution after one year of drift. The percentage of *Sargassum* beaching in each coastal 50km cell is computed with respect to the initial quantity of *Sargassum*. Percentages were first computed for each simulation of Exp2, then averaged.

Supplementary materials:

SM1 MODIS processing to AFAI
SM2 Movie: Top panel. 6-hourly positions (black dots) of the surface drifter #64501650 from aoml.noaa.gov (Lumpkin & Centurioni 2019) from November 2nd to December 21st 2017, in the Western Tropical Atlantic. This drifter lost its drogue on July 8th. Bottom panel. Evolution of the daily AFAI in a 2x2° neighborhood of the drifter. AFAI values above 210^{-4} (red color) are *Sargassum* aggregations while masked areas are in white. Only scenes with sufficient coverage are plotted. Drifter positions are overlaid as black dots.

10

Lumpkin, Rick; Centurioni, Luca (2019). Global Drifter Program quality-controlled 6-hour interpolated data from ocean surface drifting buoys. Subset 2017, Tropical Atlantic. NOAA National Centers for Environmental Information. Dataset. https://doi.org/10.25921/7ntx-z961. Accessed 2018/03/01.

1
2
3
4
5
6
7
8
9
10
11
12
13
14
15
16
17
18
19
20
21
22
23
24
25
26
27
28
29
30
31
32
33
34
35
36
37
38
39
40
41
42
43
44
45
46
47
48
49
50
51
52
53
54
55
56
57
58
59
60
61
62
63
64
65

Figure 1
Click here to download high resolution image
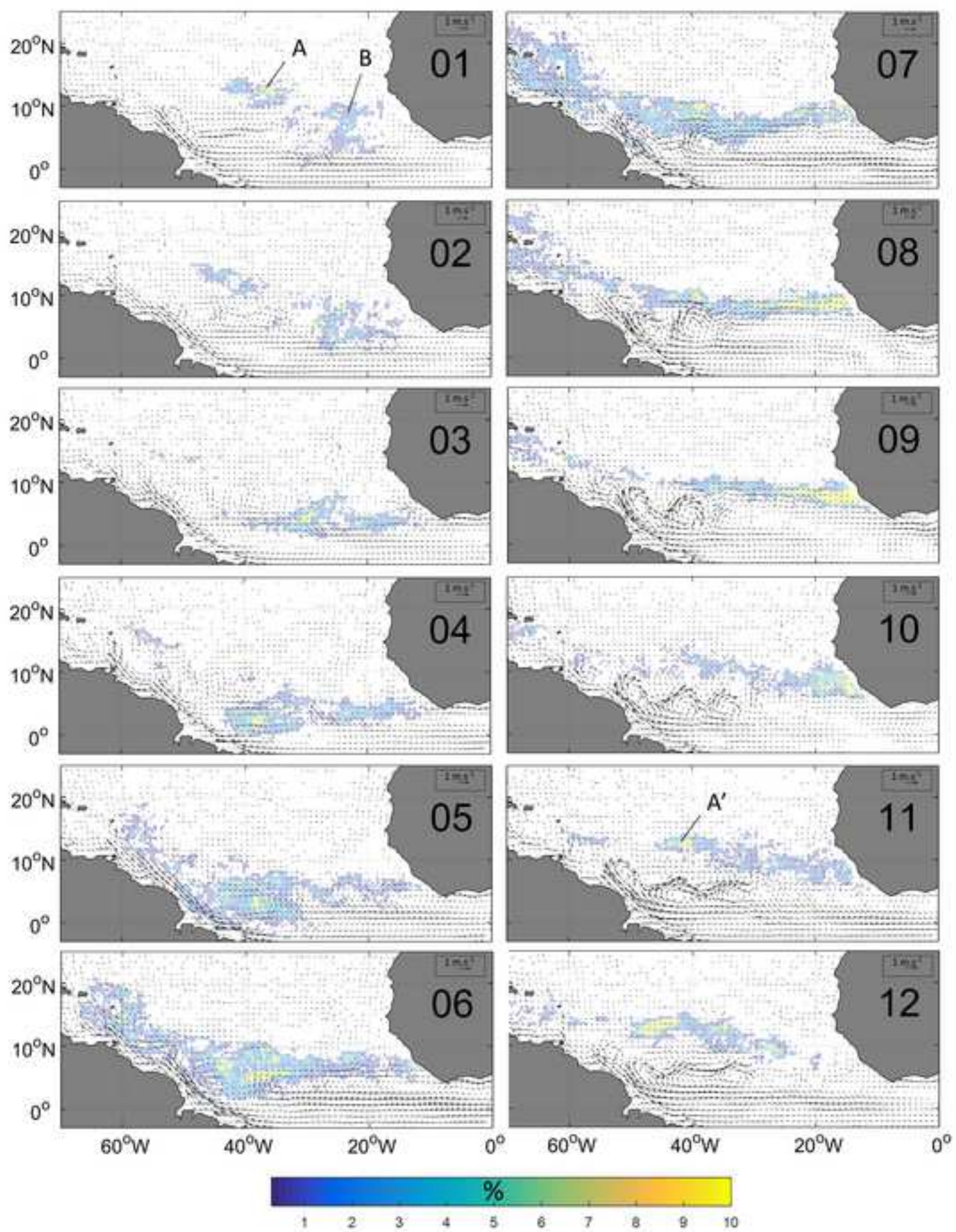
Figure 2
Click here to download high resolution image
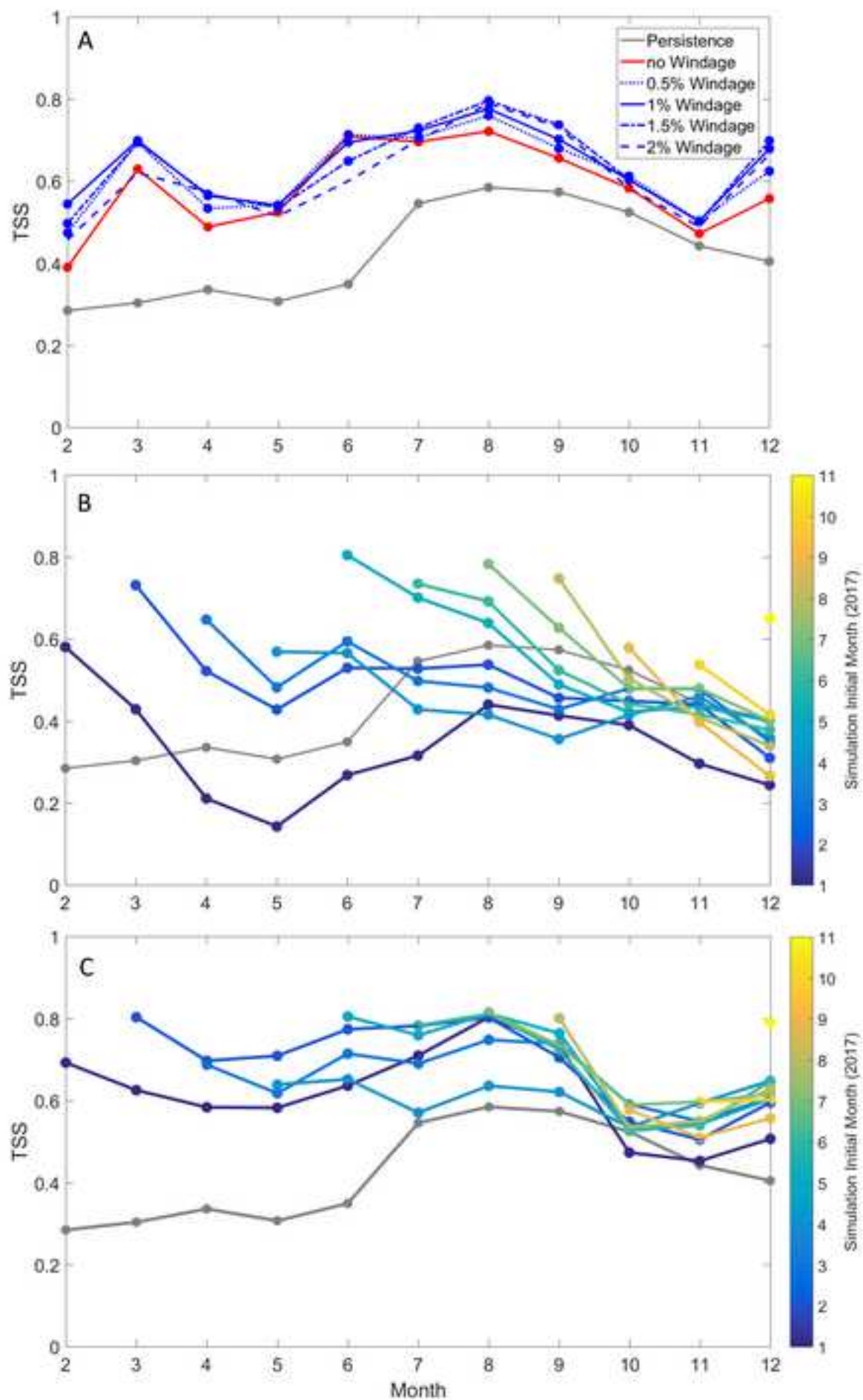
Figure 3
Click here to download high resolution image
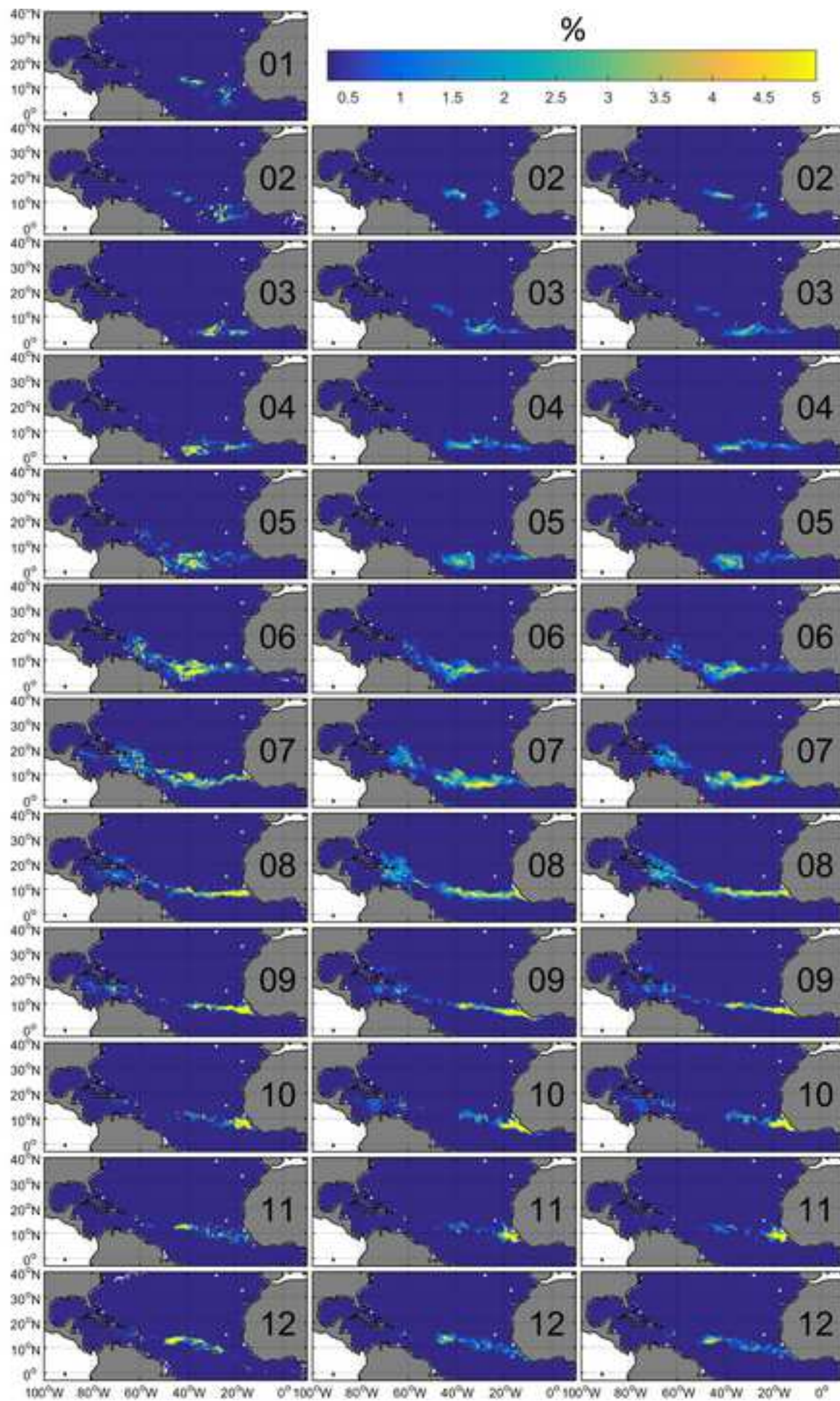
Figure 4
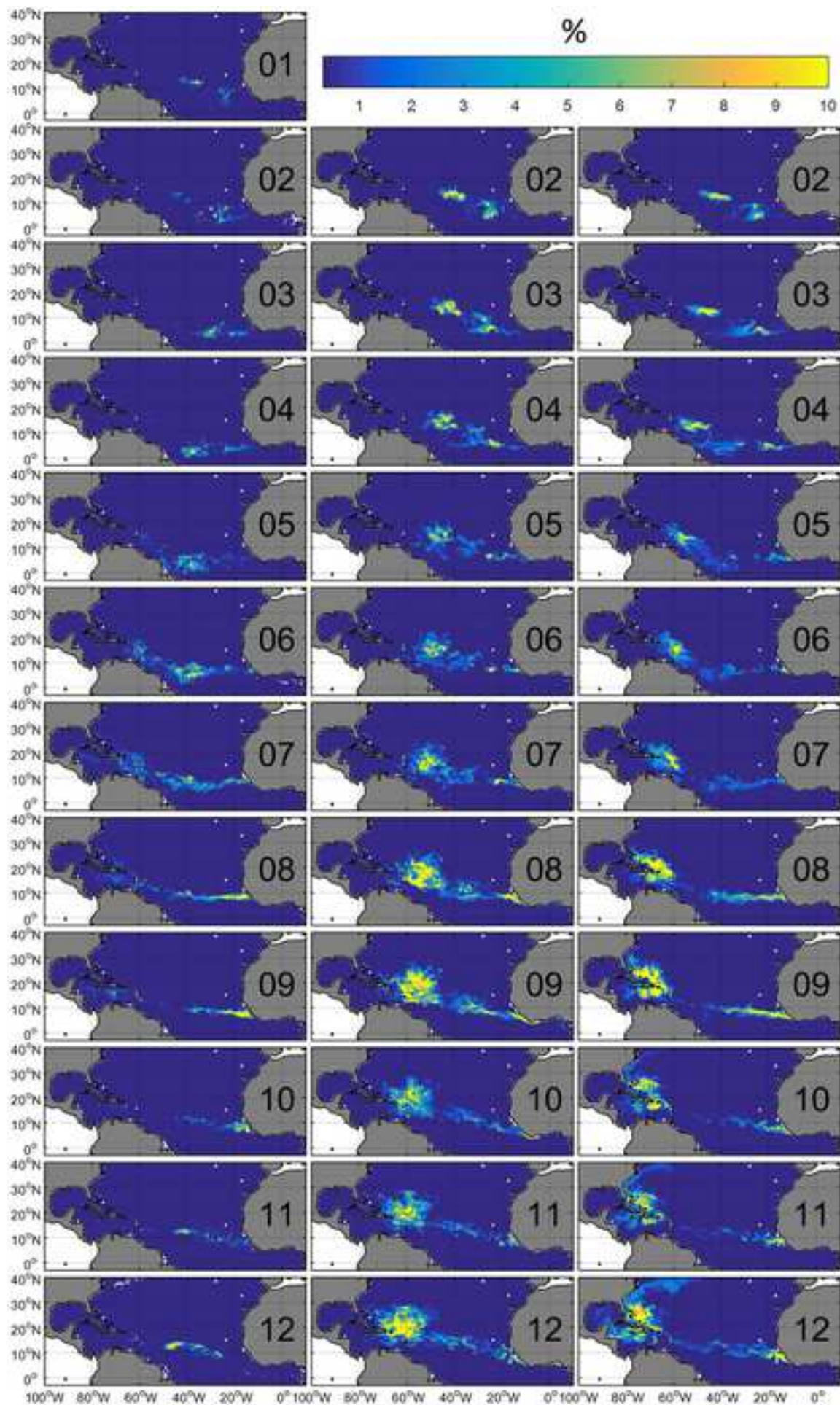
Figure 5
Click here to download high resolution image
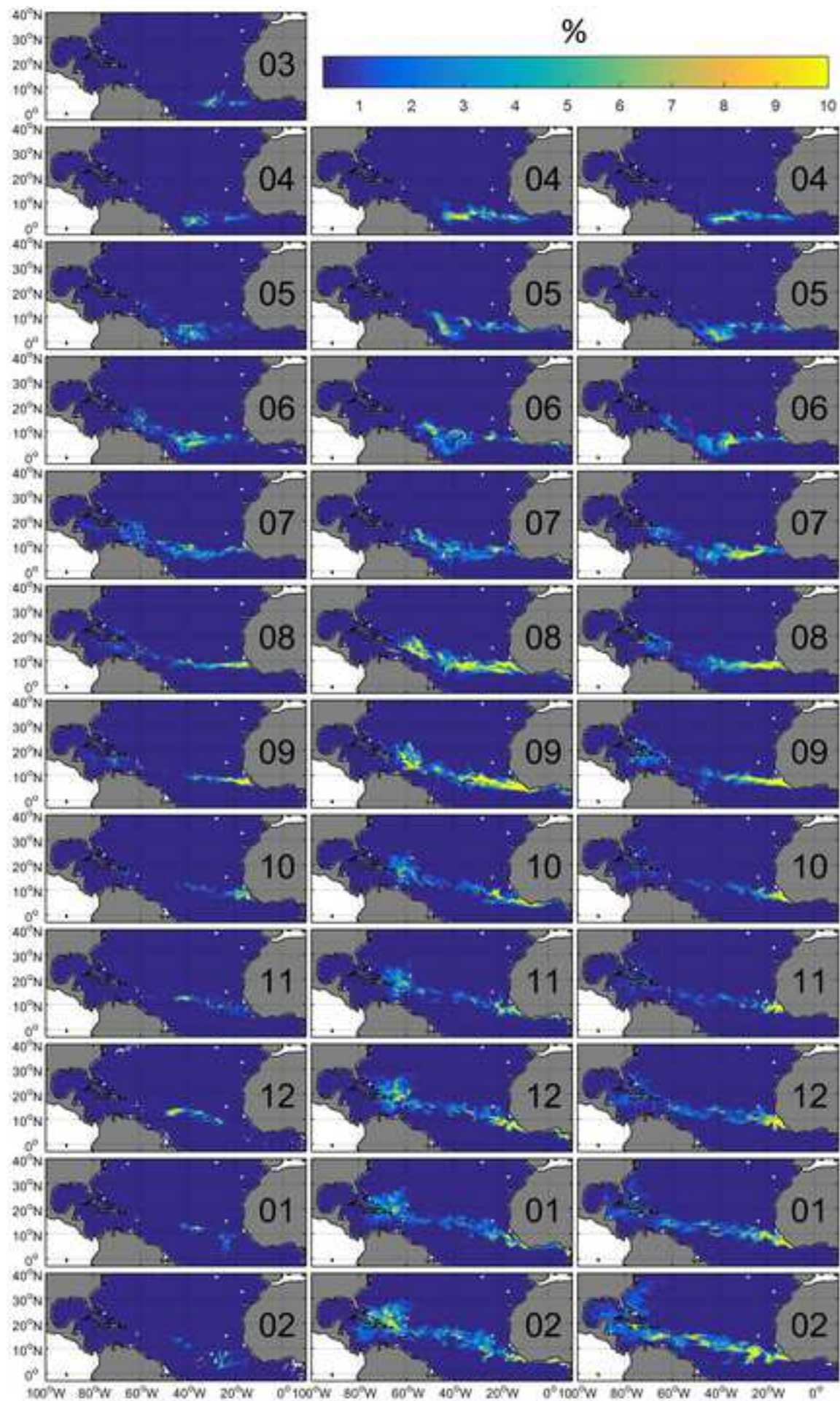
Figure 6
Click here to download high resolution image
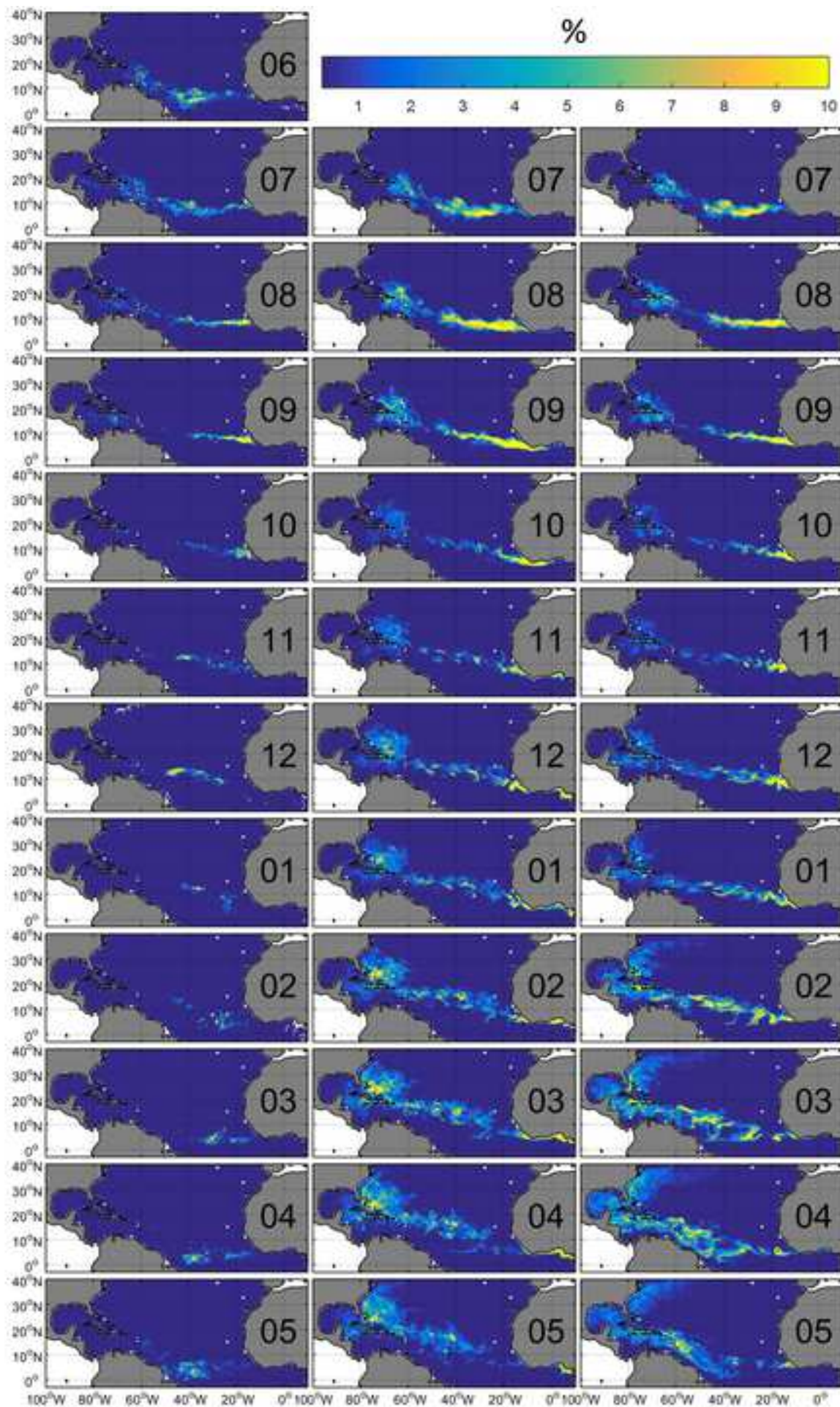
Figure 7
Click here to download high resolution image
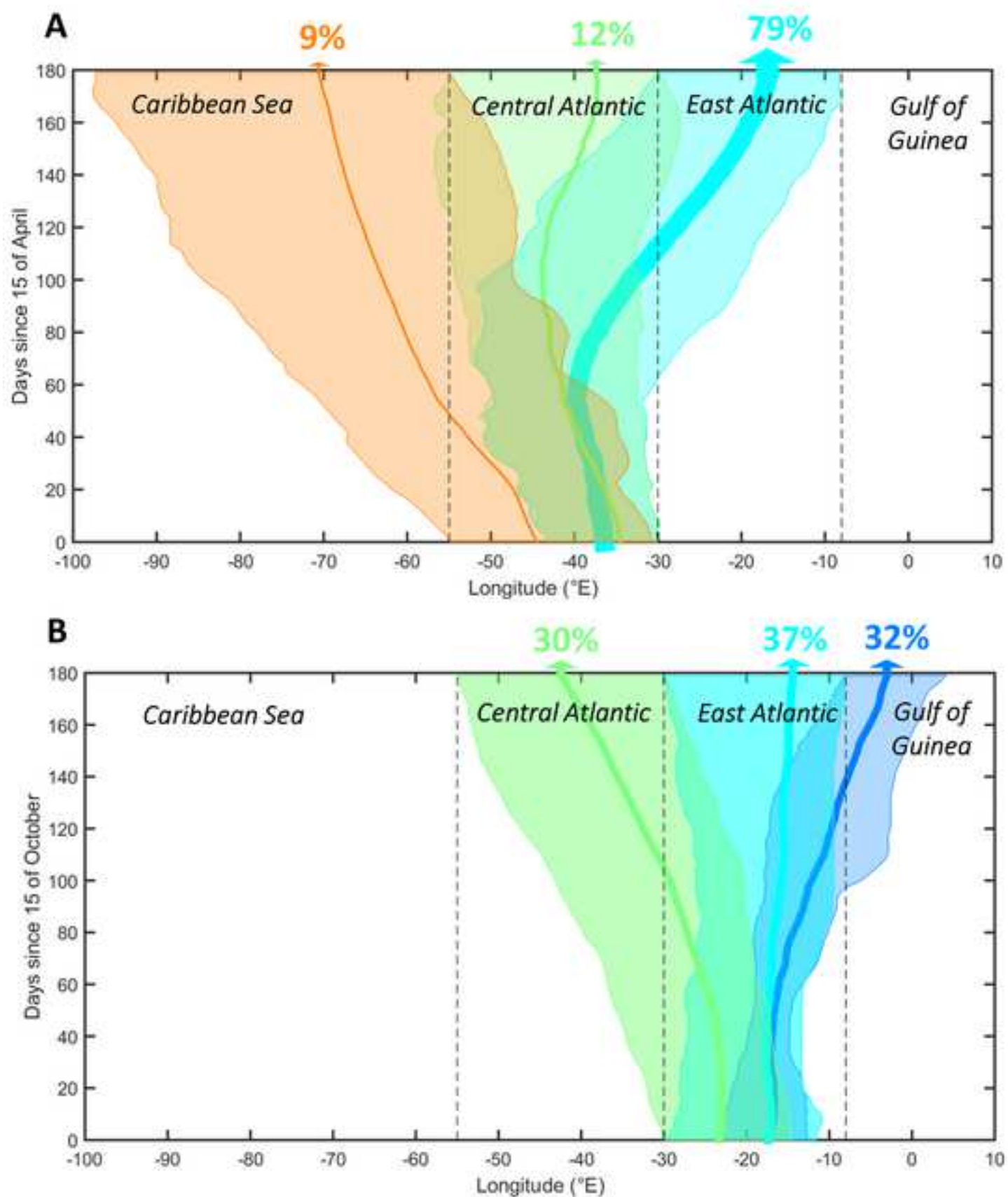
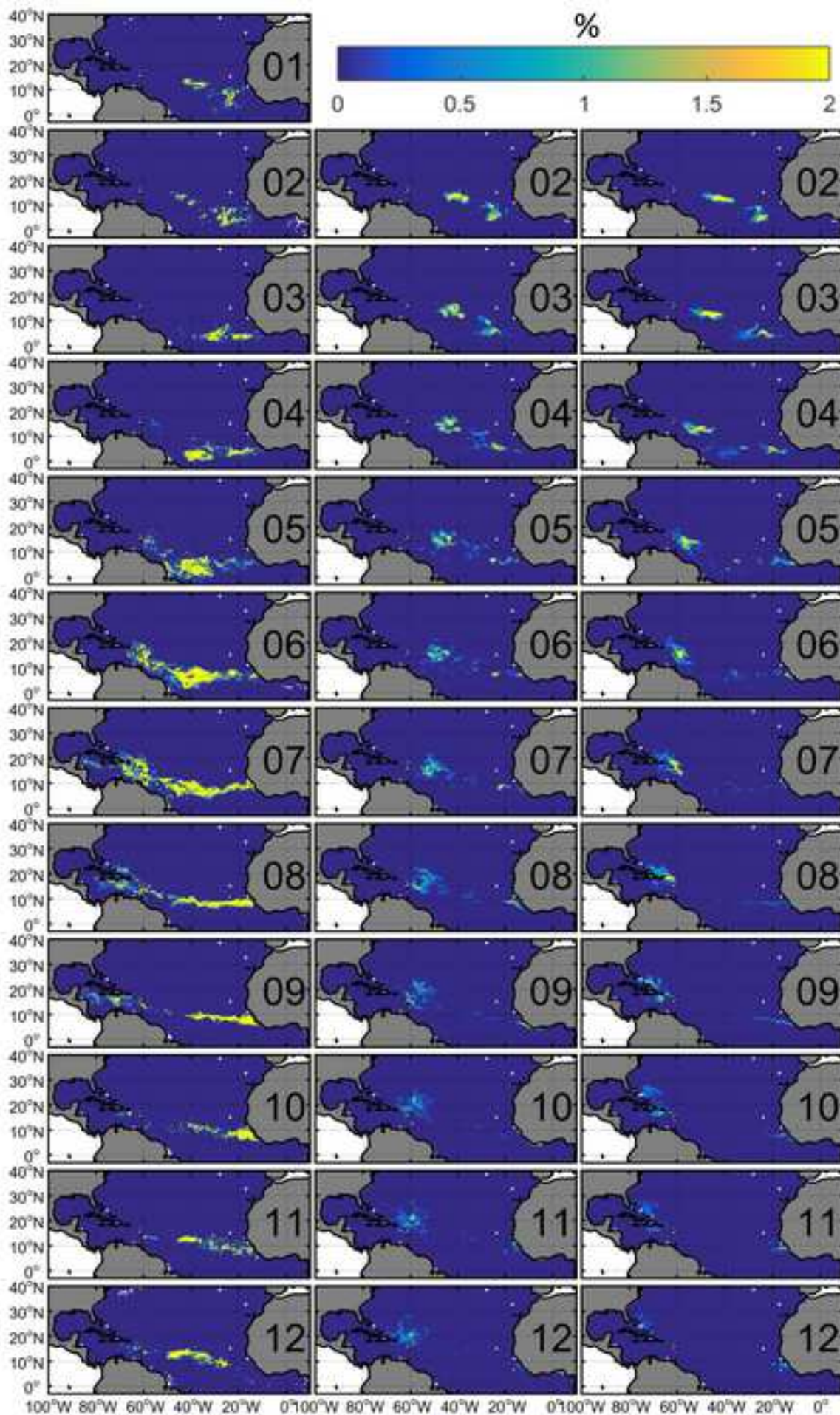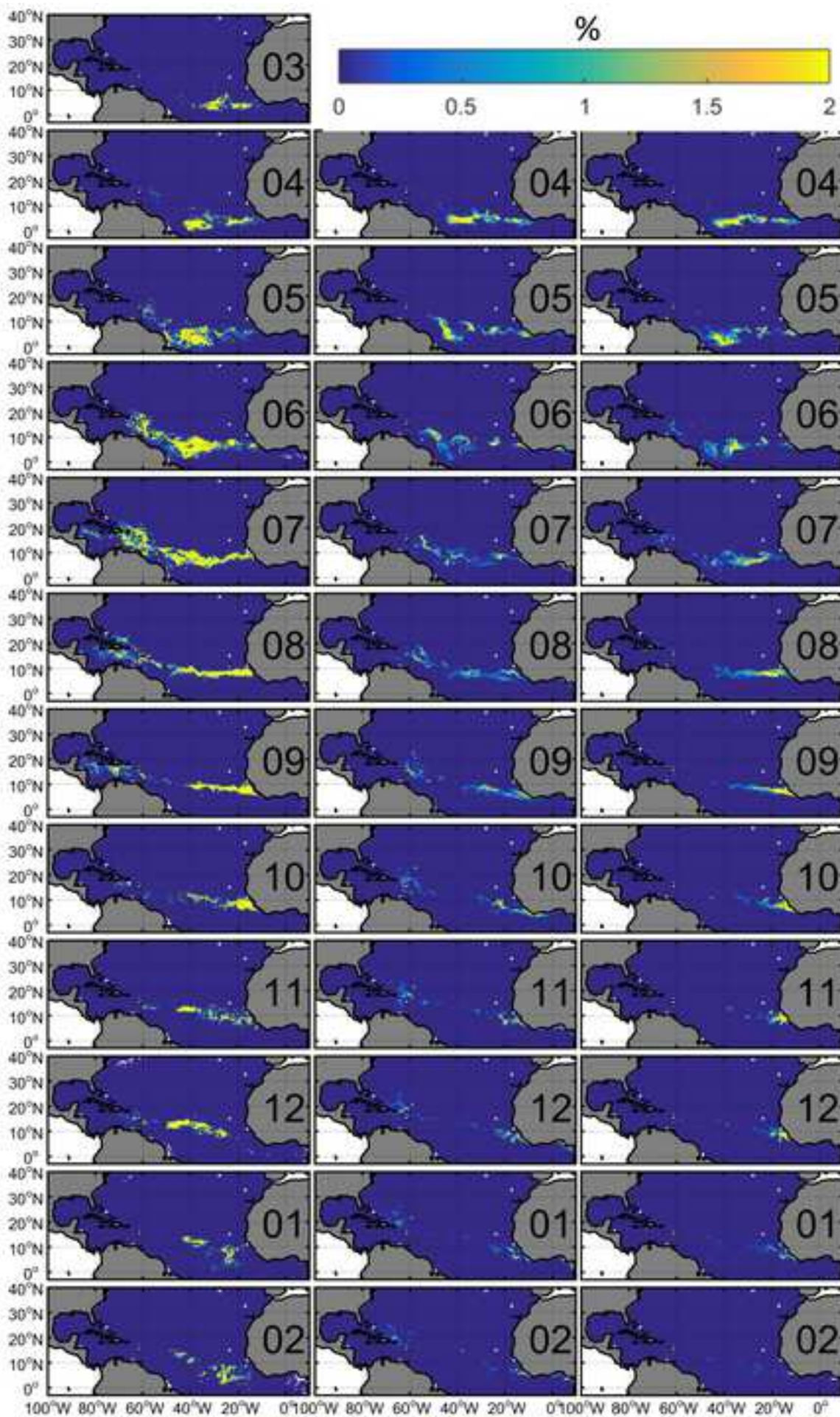**Figure 8**
[Click here to download high resolution image](#)